# Synergistic inhibition of two host factors that facilitate entry of Severe Acute Respiratory Syndrome Coronavirus 2

Alex J.B. Kreutzberger[a,b], Anwesha Sanyal[a,b], Ravi Ojha[c], Jesse D. Pyle[d], Olli Vapalahti[c,e,f], Giuseppe Balistreri[c,e] and Tom Kirchhausen[a,b,g,#]

[a] Department of Cell Biology, Harvard Medical School, 200 Longwood Av, Boston, MA 02115, USA

[b] Program in Cellular and Molecular Medicine, Boston Children's Hospital, 200 Longwood Av, Boston, MA 02115, USA

[c] Department of Virology, Faculty of Medicine, University of Helsinki, Helsinki, Finland

[d] Program in Virology, Harvard Medical School, 200 Longwood Ave, Boston, MA 02115, USA

[e] Department of Veterinary Biosciences, University of Helsinki, Helsinki, Finland

[f] Virology and Immunology, Helsinki University Hospital Diagnostic Center (HUSLAB), Helsinki, Finland

[g] Department of Pediatrics, Harvard Medical School, 200 Longwood Ave, Boston, MA 02115, USA

Running Head: Synergistic block of SARS-CoV-2 infection

#Address correspondence to Tom Kirchhausen kirchhausen@crystal.harvard.edu

## ABSTRACT

Repurposing FDA-approved inhibitors able to prevent infection by severe acute respiratory syndrome coronavirus 2 (SARS-CoV-2) could provide a rapid path to establish new therapeutic options to mitigate the effects of coronavirus disease 2019 (COVID-19). Proteolytic cleavages of the spike S protein of SARS-CoV-2, mediated by the host cell proteases cathepsin and TMPRSS2, alone or in combination, are key early activation steps required for efficient infection. The PIKfyve kinase inhibitor apilimod interferes with late endosomal viral traffic, and through an ill-defined mechanism prevents *in vitro* infection through late endosomes mediated by cathepsin. Similarly, inhibition of TMPRSS2 protease activity by camostat mesylate or nafamostat mesylate prevents infection mediated by the TMPRSS2-dependent and cathepsin-independent pathway. Here, we combined the use of apilimod with camostat mesylate or nafamostat mesylate and found an unexpected ~5-10 fold increase in their effectiveness to prevent SARS-CoV-2 infection in different cell types. Comparable synergism was observed using both, a chimeric vesicular stomatitis virus (VSV) containing S of SARS-CoV-2 (VSV-SARS-CoV-2) and SARS-CoV-2 virus. The substantial ~5 fold or more decrease of half maximal effective concentrations ($EC_{50}$ values) suggests a plausible treatment strategy based on the combined use of these inhibitors.


## IMPORTANCE

Infection by severe acute respiratory syndrome coronavirus 2 (SARS-CoV-2) is causing the coronavirus disease 2019 (COVID-2019) global pandemic. There are ongoing efforts to uncover effective antiviral agents that could mitigate the severity of the

disease by controlling the ensuing viral replication. Promising candidates include small molecules that inhibit the enzymatic activities of host proteins, thus preventing SARS-CoV-2 entry and infection. They include Apilimod, an inhibitor of PIKfyve kinase and camostat mesylate and nafamostat mesylate, inhibitors of TMPRSS2 protease. Our research is significant for having uncovered an unexpected synergism in the effective inhibitory activity of apilimod used together with camostat mesylate or with nafamostat mesylate.

51 **INTRODUCTION**

52 Severe acute respiratory syndrome coronavirus 2 (SARS-CoV-2) infection has caused
53 the global pandemic known as coronavirus disease 2019 (COVID-2019). Currently
54 there is no widespread use of an antiviral agent against the disease, but several
55 candidates have been identified (1-6). Apilimod is currently in a clinical trial for the
56 prevention of SARS-CoV-2 infections in the United States of America (ClinicalTrails.gov
57 Identifier: NCT04446377). The TMPRSS2 protease inhibitor camostat mesylate has
58 been tested with hospitalized COVID-19 patients in Denmark (7) and is in a clinical trial
59 on adult COVID-19 patients in France (ClinicalTrails.gov Identifier: NCT04608266),
60 while the higher affinity TMPRSS2 protease inhibitor, nafamostat mesylate, is being
61 used in COVID-19 related trials in Russia (ClinicalTrials.gov Identifier: NCT04623021),
62 South Korea (ClinicalTrails.gov Identifier: NCT04418128) and Japan (8).
63

64 Targeting the entry route of SARS-CoV-2 has been particularly challenging because
65 there appear to be at least two different pathways for virus entry into cells (1). SARS-
66 CoV-2 entry is mediated by the virus spike protein (9-11) and requires the receptor
67 ACE2 in the host cell (1, 12, 13). Upon engagement of the ACE2 receptor, the spike
68 protein catalyzes fusion of the viral membrane envelope with a host cell membrane to
69 release the contents of the virus into the cytoplasm of host cells. For the spike protein
70 to facilitate this reaction, it must first be cleaved by a host cell protease (1, 10). This
71 can be accomplished by different host proteases including TMPRSS2 and TMPRSS4
72 (14), Factor Xa (15, 16), and by cathepsins during endocytosis (1). The protease
73 inhibitors E-64 and camostat mesylate target cathepsin and TMPRSS2 and inhibit

74 SARS-CoV-2 infection (1), but their low (micromolar) affinities have made them unlikely
75 candidates for clinical use. Nafamostat mesylate inhibits TMPRSS2 with a high
76 (nanomolar) affinity (2, 6). Apilimod has been shown to function in the endosomal
77 pathway by inhibiting PIKfyve kinase causing a defect in viral trafficking prior to entry (3)
78 but how this relates to the cathepsin or TMPRSS2 protease dependent pathways has
79 not been investigated.
80
81 Using a chimeric vesicular stomatitis virus (VSV) in which the attachment and fusion
82 glycoprotein G is replaced by the spike S protein of SARS-CoV-2 (VSV-SARS-CoV-2)
83 (17) we investigate inhibition of infection in different cell types known to contain different
84 levels of cathepsin and TMPRSS2 proteases. We tested combinations of the protease
85 inhibitors E-64 (cathepsin), camostat mesylate and nafamostat mesylate (TMPRSS2)
86 and the lipid kinase inhibitor apilimod (PIKfyve kinase) on VSV-SARS-CoV-2 infection of
87 multiple cell types. We observed a 5-fold synergistic effect in the infection of VSV-
88 SARS-CoV-2 by simultaneous inhibition of TMPRSS2 and PIKfyve kinase. Furthermore,
89 the synergistic inhibitory effects on infection by VSV-SARS-CoV-2 or a clinical isolate of
90 SARS-CoV-2 were observed with nanomolar concentrations of camostat mesylate and
91 apilimod. This finding suggests that a combination of inhibitors that target two different
92 host factors in the entry pathway of SARS-CoV-2 will likely be more effective than
93 targeting either alone.

## RESULTS AND DISCUSSION

### VSV-SARS2-CoV-2 infection is partially prevented by PIKfyve kinase or TMPRSS2 protease inhibitors

It has been proposed that two distinct host proteases, TMPRSS2 and cathepsin facilitate different SARS2-CoV-2 viral entry routes - cell surface or endosomal - and their abundance in different cell types may influence the entry pathway (1). To test this, we employed a panel of inhibitors on SARS-CoV-2 infection in African green monkey kidney epithelial derived VeroE6 cells poorly expressing TMPRSS2, VeroE6 cells stably expressing ectopic TMPRSS2, as well as human colon carcinoma derived Caco-2 cells and human lung derived Calu-3 cells naturally expressing TMPRSS2.

We first established the relative importance of the cathepsin-dependent route for infection of VSV-SARS-CoV-2 by determining the effect of the cathepsin inhibitor E-64 on expression of eGFP mediated by VSV-SARS-CoV-2. As summarized in the plots in Fig. 1A, we found a cell type dependence in the extent of infection block with a half maximal effective concentration ($EC_{50}$) in the ~5-10 μM range. Notably, only Vero E6 cells treated with E-64 displayed a full infection block, the result expected for cells expressing cathepsin but no TMPRSS2; in contrast, cells expressing cathepsin and TMPRSS2 (VeroE6 + TMPRRS2, Caco-2) displayed a partial block, while Calu-3 cells with minimal expression of cathepsin L (18) did not respond, as expected, to E-64 treatment (1).

117 We extended the analysis and studied the inhibitory effect by the PIKfyve kinase
118 inhibitor apilimod on VSV-SARS-CoV-2 infection (Fig. 1 B). We found that all cell types
119 shown to be sensitive to E-64 also responded to treatment with apilimod with $EC_{50}$ ~ 10
120 nM whereas Calu-3, which is insensitive to E-64 (19), did not respond. Although
121 apilimod doesn't inhibit cathepsin B or L (20), these observations are consistent with
122 potential modulation of the endosomal availability of cathepsin by the activity of PIKfyve
123 kinase (21, 22).
124
125 A similar analysis, to document the reduction of viral infection using camostat mesylate
126 to block the protease activity of TPMRSS2 (Fig. 1C) or nafamostat mesylate (Fig. 1D)
127 showed, as anticipated, no response in Vero E6 cells lacking TMPRSS2, partial
128 inhibition in Vero E6 or Caco-2 cells expressing TMPRSS2 or full inhibition in Calu-3
129 cells naturally expressing TMPRSS2 but insensitive to cathepsin inhibition.
130
131 These observations are consistent with previous results (1, 2, 6, 19) that infection by
132 VSV-SARS-CoV-2 occurred through two complementary entry pathways with different
133 importance depending on the cell type, one depending on the proteolytic activity of
134 cathepsin and the second relying of the proteolytic activity of TMPRSS2. As a negative
135 control for these experiments, we included infection by the parental VSV (Fig. 1E),
136 whose ability to infect host cells is known to be independent of the enzymatic activities
137 of cathepsin, TMPRSS2, or PIKfyve kinase (1-4, 6). As expected, none of the inhibitors
138 for these enzymes influenced the extent of VSV infectivity in any of the cells used. From

139 these results we could also exclude potential cytotoxic effects by the compounds in the
140 concentration range used.
141
142 **Synergistic prevention of VSV-SARS2-CoV-2 infection by combined use of**
143 **PIKfyve kinase and TMPRSS2 protease inhibitors**
144 Since the cathepsin and TMPRSS2-dependent activation of SARS-CoV-2 correspond to
145 complementary entry pathways thought to act independent of each other, we expected
146 an additive inhibitory effect upon their simultaneous inhibition in cells that express both
147 proteases. Indeed, VSV-CoV-2 infection of Vero E6 cells expressing cathepsin and
148 TMPRSS2 (VeroE6 +TMPRSS2) were equally inhibited ($EC_{50}$ ~ 2 μM) by camostat
149 mesylate in the absence or increasing concentrations of E-64 up to 20 μM, the
150 concentration at which E-64 maximally blocked VSV-CoV-2 infection (Fig. 2A). We used
151 SynergyFinder 2.0 (23) to compare the combined response obtained experimentally
152 with the expected outcome calculated by the Bliss synergy-scoring model. Using this
153 reference model, that considers multiplicative effect of single drugs as if they acted
154 independently (23, 24), we obtained a δ-score of 6 indicative of an additive interaction
155 between camostat and E-64. In contrast, combined use of apilimod and camostat
156 mesylate led to enhanced inhibition of VSV-CoV-2 infection with a ~ 2 fold decrease in
157 the $EC_{50}$ of camostat mesylate (from 1 to 0.4 μM) (Fig. 2B), suggestive of a synergy
158 effect.
159
160 We carried a similar set of experiments using Calu-3 cells known to be deficient in
161 Cathepsin-L (18, 25) and are poorly susceptible to infection of filoviruses mediated by

162 the cathepsin-dependent infection route (18). These cells are insensitive to inhibition by
163 of VSV-SARS-CoV-2 and SARS-CoV-2 infection by E-64 (1, 19, 26, 27) (Fig.1B) and
164 apilimod ((19, 28), Fig. 1C). While presence of E-64 did not affect the inhibition profile
165 of camostat mesylate (Fig. 2C), we detected a ~ 5-fold decrease from 1 μM to 0.2 μM in
166 the EC50 of apilimod in cells simultaneously treated with 10 μM E-64 (Fig. 2D). This
167 result was unexpected, given that infection of the Calu-3 cells by SARS-CoV-2 didn't
168 appear to be affected by apilimod ((28) and Fig. 1C).
169
170 We extended the synergy analysis to verify the effects upon simultaneous use of
171 variable amounts of apilimod and nafamostat mesylate, another inhibitor of TMPRSS2.
172 Our data also indicates enhanced infection inhibition for nafamostat mesylate with a ~
173 20-fold decrease of $EC_{50}$ from 0.02 to 0.001 μM (Fig. 3A, central panel). Simultaneous
174 treatment with apilimod and increasing amounts of nafamostat mesylate led to an
175 analogous enhanced potency of apilimod inhibition with a ~10-fold decrease of $EC_{50}$
176 from 0.01 to 0.001 μM (Fig. 3A, right panel). Formal evaluation for synergism using the
177 Bliss reference model was consistent with a synergy δ-score of 41 (a score greater than
178 10 indicates synergy (23)).
179
180 Comparable strong synergistic effects (δ-score of 34) by combined use of apilimod and
181 nafamostat mesylate were observed in Vero E6 cells expressing TMPRSS2 (Fig. 3B,
182 central and right panels) infected with VSV-SARS-CoV-2 D614G whose spike S protein
183 includes the point mutation known to increase infectivity of the native SARS-CoV-2 (29).
184 While this mutation has no effect on the virus entry mechanism or sensitivity to

185 proteases, it stabilizes the stalk region of the spike, which otherwise tend to fall apart
186 after furin cleavage between S1 and S2 (29-32).
187
188 Taken together, these synergy results highlight the unexpected non-additive
189 involvement of PIKfyve kinase activity for the functional effectiveness of TMPRSS2 to
190 mediate viral entry along the TMPRSS2 route.
191
192 **Synergistic prevention of SARS2-CoV-2 infection by combined use of PIKfyve**
193 **kinase and TMPRSS2 protease inhibitors**
194 To determine whether SARS-CoV-2 virus also display an enhanced block of infection
195 upon combined use of apilimod and camostat mesylate we infected Caco-2 cells
196 ectopically expressing hACE2, the main receptor for SARS-CoV-2. This cell line was
197 created as a way to enhance the susceptibility of Caco-2 to infection by SARS-CoV-2
198 since the parental cells express low endogenous levels of ACE2 (33); successful
199 infection was scored 18 hrs post infection by the appearance of viral N protein using
200 immunofluorescence microscopy (Fig. 4, left panel). The inhibitory $EC_{50}$ of camostat
201 mesylate decreased ~ 6 fold from 0.6 to 0.1 μM when used together with apilimod, (Fig.
202 4, right panel). This observation extends our results from VSV-SARS-CoV-2 chimeras to
203 SARS-CoV-2 virus, and illustrates that combined chemical inhibition of PIKfyve kinase
204 and TMPRSS2 protease activities is likely to also prevent SARS-CoV-2 infection with
205 strong synergy.
206
207 **Final remarks**

208 According to our present understanding of early steps necessary for successful
209 infection, SARS-CoV-2 would enter cells using two main redundant routes, each
210 requiring cleavage of the viral S spike protein, one dependent on the proteolytic
211 activities of members of the cathepsin family, the other requiring proteolysis by
212 TMPRSS2 or similar transmembrane-serine proteases. Expression level of these
213 proteases depends on cell type and hence their relative importance to support
214 successful infection would hinge in part on their relative expression. Cathepsin is
215 primarily found in late endosomes or lysosomes and requires low pH for optimal
216 enzymatic activity; for these reasons it has been proposed that SARS-CoV-2 entry
217 occurs from the endolysosomal compartment (34, 35). In contrast, TMPRSS2 is thought
218 to be at the cell surface (36) and its optimal proteolytic activity is pH independent (37);
219 hence it has been inferred that TMPRSS2 cleavage of spike S protein occurs on virions
220 at the plasma membrane from which viral entry is then assumed to occur (1).
221
222 Not surprising for protease inhibitors with different targets, combined inhibition of the
223 enzymatic activities of cathepsin and TMPRSS2 by the respective protease inhibitors E-
224 64 and camostat mesylate led to additive prevention of infection by
225 SARS-CoV-2 (1) and by the VSV-SARS-CoV-2 chimera (this study).
226
227 Apilimod specifically inhibits PIKfyve kinase thereby preventing its ability to generate
228 PI(3,5)P2, a key phosphoinositide required to modulate the function of a number of
229 proteins involved in late endosomal traffic (3, 21, 38, 39). While it is now well
230 established that interference with PIKfyve kinase prevents infection of a selected group

231 of viruses including, Ebola (20) and VSV-Ebola (3), Marburg (20), VSV-SARS-CoV-2 (3)
232 and native SARS-CoV-2 (3-5), the molecular mechanism responsible for the
233 interference remains to be determined. Apilimod demonstrated anti-Ebola infection
234 synergy with clomiphene cytrate (δ-score of 23.8; re-calculated from data in Fig. 1B of
235 (40) using the Bliss reference model (23)) and with other drugs that interfere by
236 unknown mechanisms with Ebola entry in late endosomes (40).
237
238 The strong synergism we described in the laboratory setting for single cell types upon
239 combined use of the PIKfyve kinase and TMPRSS2 inhibitors highlights the potential
240 clinical advantage of using a similar strategy to ameliorate the viral load and potentially
241 reduce the risk to COVID-19 in patients infected with SARS-CoV-2 based on
242 simultaneous inhibition of these enzymes. Variants of apilimod and camostat rendered
243 more soluble by mesylate modification are orally administered inhibitors presently under
244 clinical trial dispensed alone for various ailments including COVID-19 (7, 41, 42). More
245 soluble nafamostat mesylate has been administered intravenously to treat COVID-19
246 patients (8). We presently don't know how efficiently these inhibitors could reach the
247 nasopharyngeal and lung tissues; nevertheless, we surmise that combined use in
248 individuals of these PIKfyve and TMPRSS2 inhibitors might also manifest ~5-10 fold
249 increase in inhibitor efficiency in the relevant target cells similar to that observed in the
250 laboratory setting, and hence be advantageous for treatment.

251 **FIGURE LEGENDS**

252 **Fig. 1. Protease inhibitors E-64, apilimod, camostat mesylate or nafamostat**
253 **mesylate prevent infection by VSV-SARS-CoV-2 but not by VSV.**

254 **(A)** Schematic of infectivity assay for cells pretreated for 1 h or not with the inhibitors,
255 subsequently infected with VSV-SARS-CoV-2 for 1 h in the presence or absence of
256 inhibitors. The cells were incubated for another 7 h in the presence or absence of
257 inhibitors and then fixed; the percentage of cells expressing eGFP measured by
258 spinning disc confocal microscopy.

259 **(B-F)** Quantification of the number of infected cells from three independent experiments,
260 each determined from 5 fields of view containing 80-200 cells per experiment (error bars
261 show SEM) for the indicated cell types. Infected Vero **(B)** or Vero + TMPRSS2 cells **C**)
262 were analyzed 8 hpi using 0.5 μg/mL VSV-SARS-CoV-2 RNA. Infected Caco-2 **(D)** or
263 Calu-3 cells **(E**) were analyzed 8 hpi using 5 μg/mL VSV-SARS-CoV-2 RNA. Cells
264 infected with 0.075 μg/mL VSV RNA **(F)** were analyzed 6 hpi. In each case, these virus
265 concentrations and conditions of infection corresponded to an MOI of ~ 0.5.

266

267 **Fig. 2. Synergistic inhibition of VSV-SARS2-CoV-2 infection by combined use of**
268 **apilimod and camostat mesylate.**

269 Data are from infection results using VSV-SARS2-CoV-2 obtained with different cell
270 types in the absence or combined presence at increasing concentrations of E-64 and
271 camostat mesylate **(A, C)** or apilimod and camostat mesylate **(B, D)**. Representative
272 maximum-Z projections views (left panels) are from whole-cell volume images obtained
273 with optical sections separated by 0.5 μm using spinning disk confocal microscopy; cells

274 were infected with 0.5 μg/mL viral RNA VSV-SARS-CoV-2 and imaged 8 hpi. Scale
275 bar: 50 μm. Corresponding quantifications of infection (right panels) are shown in the
276 plots. Each point corresponds to one independent experiment; the data represent
277 results from 5 fields of view containing 80-200 cells per experiment. Estimated $EC_{50}$'s
278 are indicated. Significance in the difference of $EC_{50}$ was determined from fitting
279 replicated experiments and using an unpaired t-test with P-values of 0.02 for **(B)** and
280 0.002 for **(C);** there was no statistically significant difference in the EC50 values for the
281 experiments reported in **(A)** or **(C)**.
282
283 **Fig. 3. Synergistic inhibition of VSV-SARS2-CoV-2 infection by combined use of**
284 **apilimod and nafamostat mesylate.**
285 Data are from infection results obtained with VeroE6 + TPRSS2 cells in the absence or
286 combined presence at increasing concentrations of apilimod and nafamostat mesylate.
287 Representative maximum-Z projections views (left panels) are from whole-cell volume
288 images obtained with optical sections separated by 0.5 μm using spinning disk confocal
289 microscopy; cells were infected with 0.5 μg/mL viral RNA VSV-SARS-CoV-2 **(A)** or 0.2
290 μg/mL VSV-SARS-CoV-2 D614G viral RNA **(B)** and imaged 8 hpi. Scale bar: 50 μm.
291 Corresponding quantifications of infection (right panels) are shown in the plots. Each
292 point corresponds to one independent experiment; the data represent results from 5
293 fields of view containing 80-200 cells per experiment. Estimated $EC_{50}$'s are indicated.
294 Both plots in the central and right panels used the same data.
295

296 **Fig. 4. Synergistic inhibition of SARS2-CoV-2 infection by combined use of**
297 **apilimod and camostat mesylate.**
298 Natural SARS-CoV-2 infection inhibition in Caco-2 + hACE2 cells (MOI = 0.5) by
299 camostat mesylate in the absence or combined presence of apilimod. Representative
300 examples of images of fixed samples stained with an antibody specific for N (red) and
301 with Hoechst DNA stain (cyan) to identify the nuclei obtained using wide field
302 epifluorescence microscopy (left panels) and corresponding quantifications of infection
303 (right panels) are shown. Each data points were from 4 independent experiments,
304 representing results from 6,000-10,000 cells per experiment. Estimated $EC_{50}$'s are
305 shown. Significance in the difference of $EC_{50}$ was determined from fitting replicated
306 experiments and using an unpaired t-test on the $EC_{50}$ values with a P-value of 0.01.

307 # MATERIAL AND METHODS

308 **Materials**

309 These reagents were purchased as indicated: Dulbecco modified Eagles Medium
310 (DMEM) supplemented with 4.5 g/L glucose, L-glutamine, and sodium pyruvate
311 (Corning, Inc., cat. 10-013-CV), fetal bovine serum (FBS, Atlanta Biologicals, cat.
312 S11150H), penicillin-streptomycin 100x solution (VWR, cat. 45000-652), camostat
313 mesylate (Sigma-Aldrich, cat. SML0057), E-64 (Santa Cruz Biotechnology, cat. sc-
314 201276), nafamostat mesylate (Cayman Chemical Company, cat. #14837), apilimod
315 (MedChem Express, cat. HY-14644), dimethyl sulfoxide (DMSO, Sigma-Aldrich, cat.
316 26855), Round cover glass #1.5, 25 mm (Cellvis cat. C8-1.5H-N), Polydimethylsiloxane
317 (PDMS, SYLGARD from Krayden, cat. DC4019862), isopropyl alcohol (VWR, cat. 9080-
318 03/MK303108), potassium hydroxide (Sigma-Aldrich, cat. 484016), wheat germ
319 agglutinin (WGA)-Alexa647 (Invitrogen, cat. W32466), paraformaldehyde (Sigma-
320 Aldrich, cat. P6148), sodium phosphate dibasic (Thermo Fisher Scientific, cat. BP329-
321 1), potassium phosphate monobasic (Sigma-Aldrich, cat. P5379), sodium chloride (EMD
322 Millipore, cat. SX0420-5), and potassium chloride (Thermo Fisher Scientific, cat. P217-
323 500), TRIS (Goldbio, cat. T-400-500), EDTA (Sigma-Aldrich, cat. E5134), sucrose
324 (Sigma-Aldrich, cat. S0389), fetal calf serum (FCS, Hyclone, cat. SH30073.03), bovine
325 serum albumin (GE Healthcare), Triton-X (Thermo Fischer, cat. 28314), Hoechst DNA
326 stain (Thermo Fischer, cat. 62249), L-glutamine (Sigma, cat. G7513), Hoechst DNA dye
327 (cat. H6021, Sigma-Aldrich), and Alexa 647 fluorescently labelled goat anti-rabbit
328 antibody (Thermo Fisher, cat. A32733).

329

330 **Purification of VSV-SARS-CoV-2 chimeras**

331 Generation of recombinant VSV (Indiana serotype) expressing eGFP (VSV-eGFP) and
332 VSV-eGFP chimeras whose glycoprotein G was replaced with either the wild type spike
333 S protein of SARS-CoV-2 Wuhan-Hu-1 strain (VSV-SARS-CoV-2) or with the point
334 mutant D614G (VSV-SARS-CoV-2 D614G) was done as described (17). Briefly, VSV
335 was grown by infection of BSRT7/5 and VSV-SARS-CoV-2 chimeras were grown by
336 infection of MA104 cells. Cells were grown in 12-18 150 mm dishes and infected at an
337 MOI of 0.01. Virus-containing supernatant was collected at 48 hours post infection. The
338 supernatant was clarified by low-speed centrifugation at 1,000 × g for 10 min at room
339 temp. An initial pellet of virus and extracellular particles was generated by centrifugation
340 in a Ti45 fixed-angle rotor at 30,000 × g (25,000 rpm) for 2 hours at 4°C. The pellet was
341 resuspended overnight in 1X NTE (100 mM NaCl, 10 mM Tris-HCl pH 7.4, 1 mM EDTA)
342 at 4°C. The resuspended pellet was layered on top of a 15% sucrose-NTE cushion and
343 subjected to ultracentrifugation in a Sw55 swinging bucket rotor at 110,000 × g (35,000
344 rpm) for 2 hours at 4°C. The supernatant was aspirated and virus pellet resuspended in
345 1X NTE overnight at 4°C. The resuspended virus pellet was separated on a 15-45%
346 sucrose-NTE gradient by ultracentrifugation in a SW55 swinging bucket rotor at 150,000
347 × g (40,000 rpm) for 1.5 hours at 4°C. The predominant light-scattering virus band was
348 observed in the lower third of the gradient and was extracted by side puncture of the
349 gradient tube. Extracted virus was diluted in 1X NTE and collected by ultracentrifugation
350 in a Ti60 fixed-angle rotor at 115,000 × g (40,000 rpm) for 2 hours at 4°C. The final
351 pellet was re-suspended overnight in 1X NTE in a volume of 0.2 to 0.5 mL depending
352 on the size of the pellet and stored at 4°C for use in subsequent imaging experiments.

353

354 **Isolation and propagation of SARS-CoV-2**

355 Human samples were obtained under the Helsinki University Hospital laboratory
356 research permit 30 HUS/32/2018 § 16. Isolation of SARS-CoV-2 from a COVID-19
357 Briefly, a nasopharyngeal swab in 500 µl of Copan UTM® Universal Transport Medium
358 was inoculated on Calu-3 cells (P1) and incubated for 1 h at 37°C, after which the
359 inoculum was removed and replaced with Minimum Essential Medium supplemented
360 with 2% FBS, L-glutamine, penicillin and streptomycin. Virus replication was determined
361 by RT-PCR for SARS-CoV-2 RdRP (43), and the infectious virus collected 48h after
362 inoculation. The P1 stock was propagated once (P2) in VeroE6+TMPRSS2, sequenced
363 and stored at -80 °C. Virus stocks were stored in DMEM, 2% FCS, 2 mM L-glutamine,
364 1% penicillin-streptomycin.

365

366 **Cell Culture**

367 VeroE6 (ATCC CRL-1586), Caco-2 (ATCC HTB-37), and Calu-3 cells (ATCC HTB-55)
368 were purchased from ATTC. VeroE6+TMPRSS2 cells were a gift from Siyan Ding (14).
369 VeroE6, VeroE6+TMPRSS2, Caco-2, and Calu-3 cells were maintained in DMEM
370 supplemented with 10% fetal bovine serum and 1% penicillin-streptomycin. VeroE6 and
371 VeroE6+TMPRSS2 cells were grown at 37°C and 5% $CO_2$ and split at a ratio of 1:10
372 every 3-4 days when cells were at ~90% confluency. Caco-2 cells were grown at 37°C
373 and 5% $CO_2$ and split at a ratio of 1:5 every 3-4 days when cells were at ~95%
374 confluency. Calu-3 cells were grown at 37°C and 7% $CO_2$ and split at a ratio of 1:3
375 every 5-6 days when cells were at ~95% confluency. BSR-T7 cells were derived from

376 BHC cells (44) and grown in DMEM supplemented with 10% FBS and 1% penicillin-
377 streptomycin. BSR-T7 were grown at 37$^{o}$C and 5% $CO_2$ and split at a ratio of 1:20 every
378 2-3 days when cells were at ~90% confluency. MA104 cells (ATCC, CRL-2378.1) were
379 grown in Media 199 supplemented with 10% FBS and 1% penicillin-streptomycin.
380 MA104 cells were grown at 37$^{o}$C and 5% $CO_2$ and split at a ratio of 1:3 every 2 days
381 when cells were at ~90% confluency. The media was changed in all cell types every 2
382 days and regularly tested for presence of mycoplasma.
383
384 Caco-2 cells stably expressing human ACE2 were generated by transduction with third
385 generation lentivirus pLenti7.3/V5 DEST ACE2-EmGFP (prepared by the cloning facility
386 Dream-Lab, Institute of Biotechnology, University of Helsinki, Helsinki, Finland; the
387 expression of Emerald GFP is driven by the SV40 promoter. Cells expressing eGFP
388 were isolated by FACS. Cells were grown in DMEM media supplemented with 10%
389 fetal calf serum, 1% penicillin-streptomycin, and 2 mM L-glutamine. Cells were kept at
390 37$^{o}$C, 5% $CO_2$, and split ever 2-4 days when ~90% confluent.
391
392 **Infection protocol for VSV and VSV-SARS-CoV-2**
393 Polydimethylsiloxane was cured by vigorously mixing with curing reagent at a ratio of 1
394 to 10. PDMS was poured into 10 cm petri dish (5 g of PDMS per plate) and incubated
395 at 90 $^{o}$C for ~4 hours. Plates were removed and stored at room temperature until use.
396 PDMS was removed from petri dish using a razor blade. 3 mm holes were punched into
397 PDMS which was cut with a blade to be ~6-10 mm. Glass slides were cleaned by
398 sonication first in isopropanol for 20 min then in 0.5M potassium hydroxide for 20 min

399 followed by extensive washing in Milli-q water. Glass was dried in an oven 60 $^{o}$C for 30
400 minutes then bonded to the PDMS by exposing PDMS and glass to air plasma at 750
401 mTorr, 30 W for 2 minutes using a PDC-001 plasma cleaner (Harrick Plasma) then
402 firmly pressing glass and PDMS together. This was followed by placing bonded glass
403 and PDMS in an oven at 90 $^{o}$C for 20 minutes. The glass cover slips mounted with a
404 PDMS well were then placed in 70% ethanol for 10 minutes to sterilize prior to use for
405 cell culture.
406
407 The day prior to the experiment cells were plated in PDMS wells on the glass slide
408 stored in a 6 well plate at a density to achieve ~70% confluence the day of the
409 experiment. On the day of the experiment cells were incubated with the desired
410 inhibitor concentration for 1 hour. Media was then removed and virus that had been
411 diluted into media containing the indicated inhibitor concentration was added to the well
412 in a volume of 10 μL. Media was left in the 6 well plate outside of the PDMS well at a
413 level less than the height of the PDMS well to maintain humidity and prevent
414 evaporation. After the virus was incubated with the cells for 1 hour the cells were
415 washed with media containing the indicated inhibitor and then the well was filled with
416 fresh media. At 6 hours after initiating the infection with VSV or 8 hours after initiating
417 the infection with VSV-SARS-CoV-2 media was removed and the cells were stained by
418 adding 5μg/mL WGA-Alexa647 in PBS (137 mM NaCl, 2.7 mM KCl, 8 mM $Na_2HPO_4$, 2
419 mM $KH_2PO_4$, pH 7.4) for 30 seconds at room temperature. Cells were then washed
420 with sterile PBS 2 times and then fixed with 4% paraformaldehyde in PBS. In all
421 experiment's cells were kept at 37$^{o}$C and 5% (for Vero, Vero+TMRPSS2, and Caco-2

422 cells) or 7% $CO_2$ (for Calu-3 cells) and media was pre warmed to 37ºC. Infected cells
423 were imaged using a spinning disk confocal microscope with a 40X oil objective with a
424 pixel size of 0.33 µm where 20 optical planes were taken at 0.5 µm apart for every field
425 of view (45). Cells were considered infected when they displayed a cytosolic
426 fluorescence signal from eGFP with a relative intensity of 1.4 times that of the
427 background of uninfected cells. Example images are max intensity projections of the cell
428 volume where the outline (white) line was obtained by tracing the WGA-Alexa647 signal
429 outlining the cell.
430
431 **Infection protocol for SARS-CoV-2**
432 All experiments with SARS-CoV-2 were performed in BSL3 facilities at the University of
433 Helsinki with appropriate institutional permits. Virus samples were obtained under the
434 Helsinki University Hospital laboratory research permit 30 HUS/32/2018 § 16. Virus titers
435 were determined by plaque assay in VeroE6+TMPRSS2 cells. Cells in DMEM,
436 supplemented with 10% FBS, 2 mM L-glutamine, pen/strep, 20 mM HEPES (pH 7.2 were
437 seeded 48 h before treatment at a density of 15,000 cells per well in 96-well imaging
438 plates (PerkinElmer cat. 6005182). Inhibitors, or DMSO control, were either added 60 min
439 prior to infection, or added 90 min post infection at a multiplicity of infection (MOI) 0.5
440 plaque forming units per cell. Infections were carried for 20 h at 37 °C and 5% $CO_2$. Cells
441 were then fixed with 4% paraformaldehyde in PBS for 30 min at room temperature before
442 being processed for immuno-detection of viral N protein, automated fluorescence imaging
443 and image analysis. Briefly, viral NP was detected with an in house developed rabbit
444 polyclonal antibody (33) counterstained with Alexa-647-conjugated goat anti rabbit

445 secondary antibody, and nuclear staining done using Hoechst DNA dye. Automated
446 fluorescence imaging was done using an epifluorescence high-content Molecular Device
447 Image-Xpress Nano microscope equipped with a 20x objective and a 4.7Mpixel CMOS
448 camera (pixel size 0.332 μm). Image analysis was performed with the software
449 CellProfiler-3 (www.cellprofiler.org). Automated detection of nuclei was obtained using
450 the Otsu algorithm inbuilt in the software. To automatically identify infected cells, an area
451 surrounding each nucleus (5 pixels expansion of the nuclear area) was used to estimate
452 the fluorescence intensity of the viral NP immuno labeled protein, using an intensity
453 threshold such that less than 0.01% of positive cells were detected in non-infected wells.
454

455 **Statistical analysis**

456 The significance of response (synergy δ-score) upon combined use of two drugs (Fig. 3)
457 was calculated using the Bliss reference model for combination of two drugs incorporated
458 in the stand-alone web-application SynergyFind v2 (23). This model assumes a stochastic
459 process in which the effects of two drugs act independently. δ-score values between -10
460 and 10 suggest an additive interaction; δ-scores larger than 10 suggest the interaction is
461 synergistic.
462

463 The $EC5_{50}$ values in Figures 2 B, C and Figure 4 were obtained from replicate
464 determinations fitted using Igor Pro (REF). An unpaired T-test was then used to
465 determine the statistical significance in the difference in the values of $EC_{50}$ of camostat
466 mesylate as a function of apilimod.

467 **AUTHOR CONTRIBUTIONS**

468 We thank Sean Whelan for comments and suggestions. Alex J.B. Kreutzberger carried
469 out all the experiments in Figs. 1-3. Ravi Ojha and Giuseppe Balistreri carried out the
470 experiments in Fig. 4. Anwesha Sanyal maintained the cells lines and assisted with
471 infectivity assays. Ravi Ojha generated Caco2-ACE2+EmGFP cells and propagated
472 SARS-CoV-2 virus under the supervision of Olli Vapalahti. Jesse Pyle generated the
473 stocks of VSV-SARS-CoV-2 chimeras. We thank Tegy John Vadakkan for maintaining
474 the spinning disc confocal microscope. This research was supported by a NIH
475 Maximizing Investigators' Research Award (MIRA) GM130386, by research grants from
476 the Danish Technical University and SANA and unrestricted funds from IONIS to T.K;
477 Harvard Virology Program, NIH training Grant T32 AI07245 postdoctoral fellowship to
478 A.J.B.K.; by an Academy of Finland research grant 336490 by the Jane and Aatos
479 Erkko Foundation, by the EU Horizon 2020 program VEO 874735, and by Helsinki
480 University Hospital Funds TYH2018322 to O.V; by a research grant from the Academy
481 of Finland grant 318434 and private funds supporting COVID-19 research to G.B.; by
482 the University of Helsinki graduate program in Microbiology and Biotechnology to R.O.
483 Tom Kirchhausen and Alex J.B. Kreutzberger were responsible for the overall design of
484 the study; Tom Kirchhausen and Alex Kreutzberger drafted the manuscript; all authors
485 commented on the manuscript.

## REFERENCES


1. Hoffmann M, Kleine-Weber H, Schroeder S, Kruger N, Herrler T, Erichsen S, Schiergens TS, Herrler G, Wu NH, Nitsche A, Muller MA, Drosten C, Pohlmann S. 2020. SARS-CoV-2 Cell Entry Depends on ACE2 and TMPRSS2 and Is Blocked by a Clinically Proven Protease Inhibitor. Cell 181:271-280 e8.
2. Hoffmann M, Schroeder S, Kleine-Weber H, Muller MA, Drosten C, Pohlmann S. 2020. Nafamostat Mesylate Blocks Activation of SARS-CoV-2: New Treatment Option for COVID-19. Antimicrob Agents Chemother 64.
3. Kang YL, Chou YY, Rothlauf PW, Liu Z, Soh TK, Cureton D, Case JB, Chen RE, Diamond MS, Whelan SPJ, Kirchhausen T. 2020. Inhibition of PIKfyve kinase prevents infection by Zaire ebolavirus and SARS-CoV-2. Proc Natl Acad Sci U S A 117:20803-20813.
4. Ou X, Liu Y, Lei X, Li P, Mi D, Ren L, Guo L, Guo R, Chen T, Hu J, Xiang Z, Mu Z, Chen X, Chen J, Hu K, Jin Q, Wang J, Qian Z. 2020. Characterization of spike glycoprotein of SARS-CoV-2 on virus entry and its immune cross-reactivity with SARS-CoV. Nat Commun 11:1620.
5. Riva L, Yuan S, Yin X, Martin-Sancho L, Matsunaga N, Pache L, Burgstaller-Muehlbacher S, De Jesus PD, Teriete P, Hull MV, Chang MW, Chan JF, Cao J, Poon VK, Herbert KM, Cheng K, Nguyen TH, Rubanov A, Pu Y, Nguyen C, Choi A, Rathnasinghe R, Schotsaert M, Miorin L, Dejosez M, Zwaka TP, Sit KY, Martinez-Sobrido L, Liu WC, White KM, Chapman ME, Lendy EK, Glynne RJ, Albrecht R, Ruppin E, Mesecar AD, Johnson JR, Benner C, Sun R, Schultz PG, Su AI, Garcia-Sastre A, Chatterjee AK, Yuen KY, Chanda SK. 2020. Discovery of SARS-CoV-2 antiviral drugs through large-scale compound repurposing. Nature 586:113-119.
6. Yamamoto M, Kiso M, Sakai-Tagawa Y, Iwatsuki-Horimoto K, Imai M, Takeda M, Kinoshita N, Ohmagari N, Gohda J, Semba K, Matsuda Z, Kawaguchi Y, Kawaoka Y, Inoue JI. 2020. The Anticoagulant Nafamostat Potently Inhibits SARS-CoV-2 S Protein-Mediated Fusion in a Cell Fusion Assay System and Viral Infection In Vitro in a Cell-Type-Dependent Manner. Viruses 12.
7. Gunst JD, Staerke NB, Pahus MH, Kristensen LH, Bodilsen J, Lohse N, Dalgaard LS, Bronnum D, Frobert O, Honge B, Johansen IS, Monrad I, Erikstrup C, Rosendal R, Vilstrup E, Mariager T, Bove DG, Offersen R, Shakar S, Cajander S, Jorgensen NP, Sritharan SS, Breining P, Jespersen S, Mortensen KL, Jensen ML, Kolte L, Frattari GS, Larsen CS, Storgaard M, Nielsen LP, Tolstrup M, Saedder EA, Ostergaard LJ, Ngo HTT, Jensen MH, Hojen JF, Kjolby M, Sogaard OS. 2021. Efficacy of the TMPRSS2 inhibitor camostat mesilate in patients hospitalized with Covid-19-a double-blind randomized controlled trial. EClinicalMedicine doi:10.1016/j.eclinm.2021.100849:100849.
8. Doi K, Ikeda M, Hayase N, Moriya K, Morimura N, Group C-US. 2020. Nafamostat mesylate treatment in combination with favipiravir for patients critically ill with Covid-19: a case series. Crit Care 24:392.
9. Huang Y, Yang C, Xu XF, Xu W, Liu SW. 2020. Structural and functional properties of SARS-CoV-2 spike protein: potential antivirus drug development for COVID-19. Acta Pharmacol Sin 41:1141-1149.

10. Shang J, Wan Y, Luo C, Ye G, Geng Q, Auerbach A, Li F. 2020. Cell entry mechanisms of SARS-CoV-2. Proc Natl Acad Sci U S A 117:11727-11734.
11. Wrapp D, Wang N, Corbett KS, Goldsmith JA, Hsieh CL, Abiona O, Graham BS, McLellan JS. 2020. Cryo-EM structure of the 2019-nCoV spike in the prefusion conformation. Science 367:1260-1263.
12. Yan R, Zhang Y, Li Y, Xia L, Guo Y, Zhou Q. 2020. Structural basis for the recognition of SARS-CoV-2 by full-length human ACE2. Science 367:1444-1448.
13. Yang J, Petitjean SJL, Koehler M, Zhang Q, Dumitru AC, Chen W, Derclaye S, Vincent SP, Soumillion P, Alsteens D. 2020. Molecular interaction and inhibition of SARS-CoV-2 binding to the ACE2 receptor. Nat Commun 11:4541.
14. Zang R, Gomez Castro MF, McCune BT, Zeng Q, Rothlauf PW, Sonnek NM, Liu Z, Brulois KF, Wang X, Greenberg HB, Diamond MS, Ciorba MA, Whelan SPJ, Ding S. 2020. TMPRSS2 and TMPRSS4 promote SARS-CoV-2 infection of human small intestinal enterocytes. Sci Immunol 5.
15. Du L, Kao RY, Zhou Y, He Y, Zhao G, Wong C, Jiang S, Yuen KY, Jin DY, Zheng BJ. 2007. Cleavage of spike protein of SARS coronavirus by protease factor Xa is associated with viral infectivity. Biochem Biophys Res Commun 359:174-9.
16. Frydman GH, Streiff MB, Connors JM, Piazza G. 2020. The Potential Role of Coagulation Factor Xa in the Pathophysiology of COVID-19: A Role for Anticoagulants as Multimodal Therapeutic Agents. TH Open 4:e288-e299.
17. Case JB, Rothlauf PW, Chen RE, Liu Z, Zhao H, Kim AS, Bloyet LM, Zeng Q, Tahan S, Droit L, Ilagan MXG, Tartell MA, Amarasinghe G, Henderson JP, Miersch S, Ustav M, Sidhu S, Virgin HW, Wang D, Ding S, Corti D, Theel ES, Fremont DH, Diamond MS, Whelan SPJ. 2020. Neutralizing Antibody and Soluble ACE2 Inhibition of a Replication-Competent VSV-SARS-CoV-2 and a Clinical Isolate of SARS-CoV-2. Cell Host Microbe 28:475-485 e5.
18. Gonzalez-Hernandez M, Muller A, Hoenen T, Hoffmann M, Pohlmann S. 2019. Calu-3cells are largely resistant to entry driven by filovirus glycoproteins and the entry defect can be rescued by directed expression of DC-SIGN or cathepsin L. Virology 532:22-29.
19. Dittmar M, Lee JS, Whig K, Segrist E, Li M, Kamalia B, Castellana L, Ayyanathan K, Cardenas-Diaz FL, Morrisey EE, Truitt R, Yang W, Jurado K, Samby K, Ramage H, Schultz DC, Cherry S. 2021. Drug repurposing screens reveal cell-type-specific entry pathways and FDA-approved drugs active against SARS-Cov-2. Cell Rep 35:108959.
20. Nelson EA, Dyall J, Hoenen T, Barnes AB, Zhou H, Liang JY, Michelotti J, Dewey WH, DeWald LE, Bennett RS, Morris PJ, Guha R, Klumpp-Thomas C, McKnight C, Chen YC, Xu X, Wang A, Hughes E, Martin S, Thomas C, Jahrling PB, Hensley LE, Olinger GG, Jr., White JM. 2017. The phosphatidylinositol-3-phosphate 5-kinase inhibitor apilimod blocks filoviral entry and infection. PLoS Negl Trop Dis 11:e0005540.
21. Baranov MV, Bianchi F, Schirmacher A, van Aart MAC, Maassen S, Muntjewerff EM, Dingjan I, Ter Beest M, Verdoes M, Keyser SGL, Bertozzi CR, Diederichsen U, van den Bogaart G. 2019. The Phosphoinositide Kinase PIKfyve Promotes

576 Cathepsin-S-Mediated Major Histocompatibility Complex Class II Antigen
577 Presentation. iScience 11:160-177.
578 22. Gayle S, Landrette S, Beeharry N, Conrad C, Hernandez M, Beckett P, Ferguson
579 SM, Mandelkern T, Zheng M, Xu T, Rothberg J, Lichenstein H. 2017.
580 Identification of apilimod as a first-in-class PIKfyve kinase inhibitor for treatment
581 of B-cell non-Hodgkin lymphoma. Blood 129:1768-1778.
582 23. Ianevski A, Giri AK, Aittokallio T. 2020. SynergyFinder 2.0: visual analytics of
583 multi-drug combination synergies. Nucleic Acids Res 48:W488-W493.
584 24. Bliss C. 1939. The Toxicity Of Poisons Applied Jointly. Ann Appl Biol
585 doi:10.1111/j.1744-7348.1939.tb06990.x:585–615.
586 25. Park JE, Li K, Barlan A, Fehr AR, Perlman S, McCray PB, Jr., Gallagher T. 2016.
587 Proteolytic processing of Middle East respiratory syndrome coronavirus spikes
588 expands virus tropism. Proc Natl Acad Sci U S A 113:12262-12267.
589 26. Murgolo N, Therien AG, Howell B, Klein D, Koeplinger K, Lieberman LA, Adam
590 GC, Flynn J, McKenna P, Swaminathan G, Hazuda DJ, Olsen DB. 2021. SARS-
591 CoV-2 tropism, entry, replication, and propagation: Considerations for drug
592 discovery and development. PLoS Pathog 17:e1009225.
593 27. Mykytyn AZ, Breugem TI, Riesebosch S, Schipper D, van den Doel PB, Rottier
594 RJ, Lamers MM, Haagmans BL. 2021. SARS-CoV-2 entry into human airway
595 organoids is serine protease-mediated and facilitated by the multibasic cleavage
596 site. Elife 10.
597 28. J K, Uckeley Z, P D, M S, S B, PY L. 2020. Host Cell Proteases Drive Early or
598 Late SARS-CoV-2 Penetration. bioRxiv
599 doi:https://doi.org/10.1101/2020.12.22.423906.
600 29. Plante JA, Liu Y, Liu J, Xia H, Johnson BA, Lokugamage KG, Zhang X, Muruato
601 AE, Zou J, Fontes-Garfias CR, Mirchandani D, Scharton D, Bilello JP, Ku Z, An
602 Z, Kalveram B, Freiberg AN, Menachery VD, Xie X, Plante KS, Weaver SC, Shi
603 PY. 2020. Spike mutation D614G alters SARS-CoV-2 fitness. Nature
604 doi:10.1038/s41586-020-2895-3.
605 30. Gobeil SM, Janowska K, McDowell S, Mansouri K, Parks R, Manne K, Stalls V,
606 Kopp MF, Henderson R, Edwards RJ, Haynes BF, Acharya P. 2021. D614G
607 Mutation Alters SARS-CoV-2 Spike Conformation and Enhances Protease
608 Cleavage at the S1/S2 Junction. Cell Rep 34:108630.
609 31. Yurkovetskiy L, Wang X, Pascal KE, Tomkins-Tinch C, Nyalile TP, Wang Y,
610 Baum A, Diehl WE, Dauphin A, Carbone C, Veinotte K, Egri SB, Schaffner SF,
611 Lemieux JE, Munro JB, Rafique A, Barve A, Sabeti PC, Kyratsous CA, Dudkina
612 NV, Shen K, Luban J. 2020. Structural and Functional Analysis of the D614G
613 SARS-CoV-2 Spike Protein Variant. Cell 183:739-751 e8.
614 32. Zhang L, Jackson CB, Mou H, Ojha A, Peng H, Quinlan BD, Rangarajan ES, Pan
615 A, Vanderheiden A, Suthar MS, Li W, Izard T, Rader C, Farzan M, Choe H. 2020.
616 SARS-CoV-2 spike-protein D614G mutation increases virion spike density and
617 infectivity. Nat Commun 11:6013.
618 33. Cantuti-Castelvetri L, Ojha R, Pedro LD, Djannatian M, Franz J, Kuivanen S, van
619 der Meer F, Kallio K, Kaya T, Anastasina M, Smura T, Levanov L, Szirovicza L,
620 Tobi A, Kallio-Kokko H, Osterlund P, Joensuu M, Meunier FA, Butcher SJ,
621 Winkler MS, Mollenhauer B, Helenius A, Gokce O, Teesalu T, Hepojoki J,

622 Vapalahti O, Stadelmann C, Balistreri G, Simons M. 2020. Neuropilin-1 facilitates
623 SARS-CoV-2 cell entry and infectivity. Science 370:856-860.
624 34. Bayati A, Kumar R, Francis V, McPherson PS. 2021. SARS-CoV-2 infects cells
625 following viral entry via clathrin-mediated endocytosis. J Biol Chem
626 doi:10.1016/j.jbc.2021.100306:100306.
627 35. Khan N, Chen X, Geiger JD. 2020. Role of Endolysosomes in Severe Acute
628 Respiratory Syndrome Coronavirus-2 Infection and Coronavirus Disease 2019
629 Pathogenesis: Implications for Potential Treatments. Front Pharmacol
630 11:595888.
631 36. Uhlen M, Fagerberg L, Hallstrom BM, Lindskog C, Oksvold P, Mardinoglu A,
632 Sivertsson A, Kampf C, Sjostedt E, Asplund A, Olsson I, Edlund K, Lundberg E,
633 Navani S, Szigyarto CA, Odeberg J, Djureinovic D, Takanen JO, Hober S, Alm T,
634 Edqvist PH, Berling H, Tegel H, Mulder J, Rockberg J, Nilsson P, Schwenk JM,
635 Hamsten M, von Feilitzen K, Forsberg M, Persson L, Johansson F, Zwahlen M,
636 von Heijne G, Nielsen J, Ponten F. 2015. Proteomics. Tissue-based map of the
637 human proteome. Science 347:1260419.
638 37. Glowacka I, Bertram S, Muller MA, Allen P, Soilleux E, Pfefferle S, Steffen I,
639 Tsegaye TS, He Y, Gnirss K, Niemeyer D, Schneider H, Drosten C, Pohlmann S.
640 2011. Evidence that TMPRSS2 activates the severe acute respiratory syndrome
641 coronavirus spike protein for membrane fusion and reduces viral control by the
642 humoral immune response. J Virol 85:4122-34.
643 38. de Lartigue J, Polson H, Feldman M, Shokat K, Tooze SA, Urbe S, Clague MJ.
644 2009. PIKfyve regulation of endosome-linked pathways. Traffic 10:883-93.
645 39. Kim GH, Dayam RM, Prashar A, Terebiznik M, Botelho RJ. 2014. PIKfyve
646 inhibition interferes with phagosome and endosome maturation in macrophages.
647 Traffic 15:1143-63.
648 40. Dyall J, Nelson EA, DeWald LE, Guha R, Hart BJ, Zhou H, Postnikova E, Logue
649 J, Vargas WM, Gross R, Michelotti J, Deiuliis N, Bennett RS, Crozier I, Holbrook
650 MR, Morris PJ, Klumpp-Thomas C, McKnight C, Mierzwa T, Shinn P, Glass PJ,
651 Johansen LM, Jahrling PB, Hensley LE, Olinger GG, Jr., Thomas C, White JM.
652 2018. Identification of Combinations of Approved Drugs With Synergistic Activity
653 Against Ebola Virus in Cell Cultures. J Infect Dis 218:S672-S678.
654 41. Billich A. 2007. Drug evaluation: apilimod, an oral IL-12/IL-23 inhibitor for the
655 treatment of autoimmune diseases and common variable immunodeficiency.
656 IDrugs 10:53-9.
657 42. Uno Y. 2020. Camostat mesilate therapy for COVID-19. Intern Emerg Med
658 15:1577-1578.
659 43. Corman VM, Landt O, Kaiser M, Molenkamp R, Meijer A, Chu DK, Bleicker T,
660 Brunink S, Schneider J, Schmidt ML, Mulders DG, Haagmans BL, van der Veer
661 B, van den Brink S, Wijsman L, Goderski G, Romette JL, Ellis J, Zambon M,
662 Peiris M, Goossens H, Reusken C, Koopmans MP, Drosten C. 2020. Detection
663 of 2019 novel coronavirus (2019-nCoV) by real-time RT-PCR. Euro Surveill 25.
664 44. Buchholz UJ, Finke S, Conzelmann KK. 1999. Generation of bovine respiratory
665 syncytial virus (BRSV) from cDNA: BRSV NS2 is not essential for virus
666 replication in tissue culture, and the human RSV leader region acts as a
667 functional BRSV genome promoter. J Virol 73:251-9.

668 45. Cocucci E, Aguet F, Boulant S, Kirchhausen T. 2012. The first five seconds in the
669 life of a clathrin-coated pit. Cell 150:495-507.
670

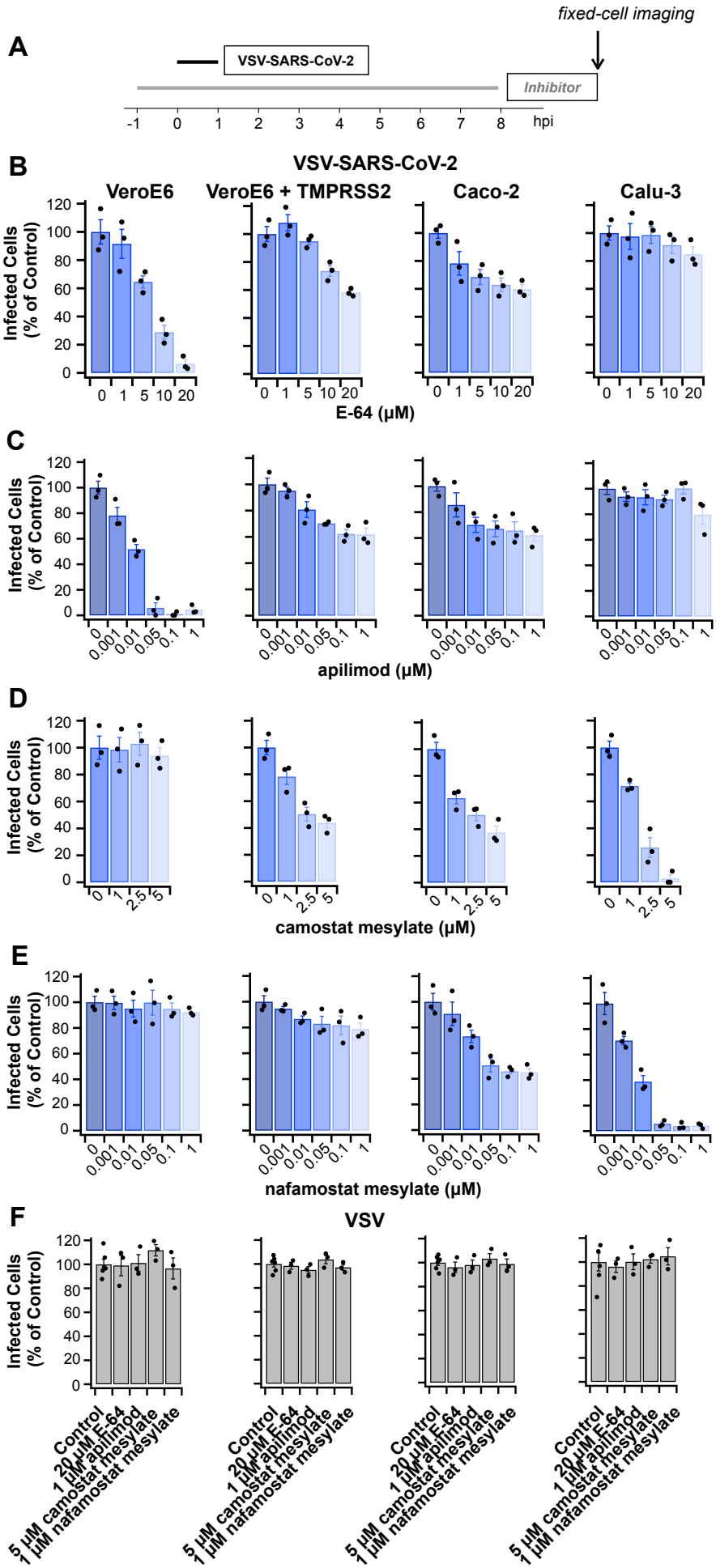
A
fixed-cell imaging
VSV-SARS-CoV-2
Inhibitor
-1 0 1 2 3 4 5 6 7 8 hpi
B
VSV-SARS-CoV-2
VeroE6
VeroE6 + TMPRSS2
Caco-2
Calu-3
Infected Cells (% of Control)
0 1 5 10 20
E-64 (μM)
C
0 0.001 0.01 0.05 0.1 1
apilimod (μM)
D
0 1 2.5 5
camostat mesylate (μM)
E
nafamostat mesylate (μM)
F
VSV
Control
20 μM E-64
1 μM apilimod
5 μM camostat mesylate
1 μM nafamostat mesylate

**Figure 1**

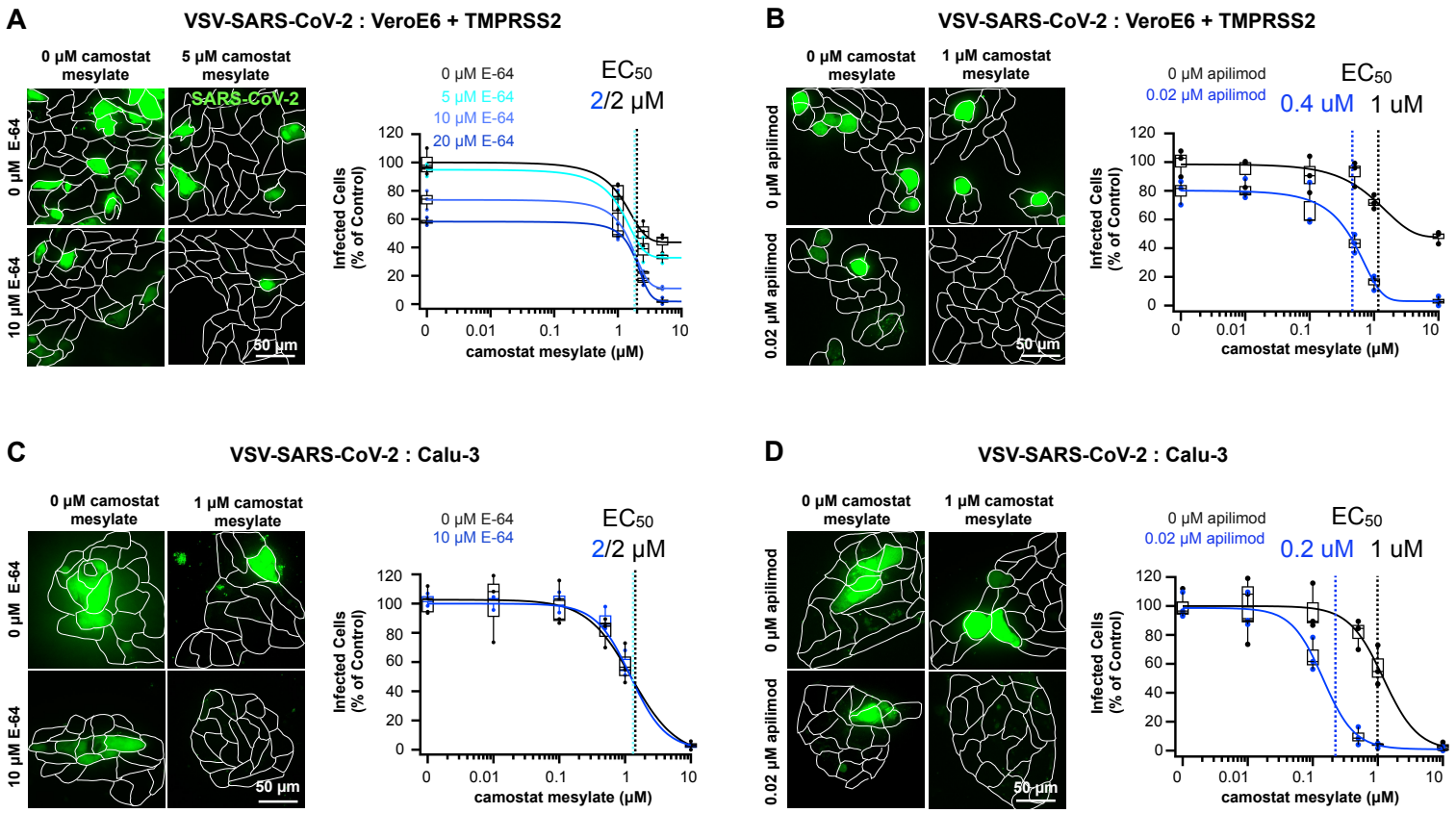
A
VSV-SARS-CoV-2 : VeroE6 + TMPRSS2
0 µM camostat mesylate
5 µM camostat mesylate
0 µM E-64
10 µM E-64
SARS-CoV-2
50 µm
0 µM E-64
5 µM E-64
10 µM E-64
20 µM E-64
EC50
2/2 µM
Infected Cells (% of Control)
camostat mesylate (µM)
B
VSV-SARS-CoV-2 : VeroE6 + TMPRSS2
0 µM camostat mesylate
1 µM camostat mesylate
0 µM apilimod
0.02 µM apilimod
50 µm
0 µM apilimod
0.02 µM apilimod
EC50
0.4 uM
1 uM
Infected Cells (% of Control)
camostat mesylate (µM)
C
VSV-SARS-CoV-2 : Calu-3
0 µM camostat mesylate
1 µM camostat mesylate
0 µM E-64
10 µM E-64
50 µm
0 µM E-64
10 µM E-64
EC50
2/2 µM
Infected Cells (% of Control)
camostat mesylate (µM)
D
VSV-SARS-CoV-2 : Calu-3
0 µM camostat mesylate
1 µM camostat mesylate
0 µM apilimod
0.02 µM apilimod
50 µm
0 µM apilimod
0.02 µM apilimod
EC50
0.2 uM
1 uM
Infected Cells (% of Control)
camostat mesylate (µM)

**Figure 2**

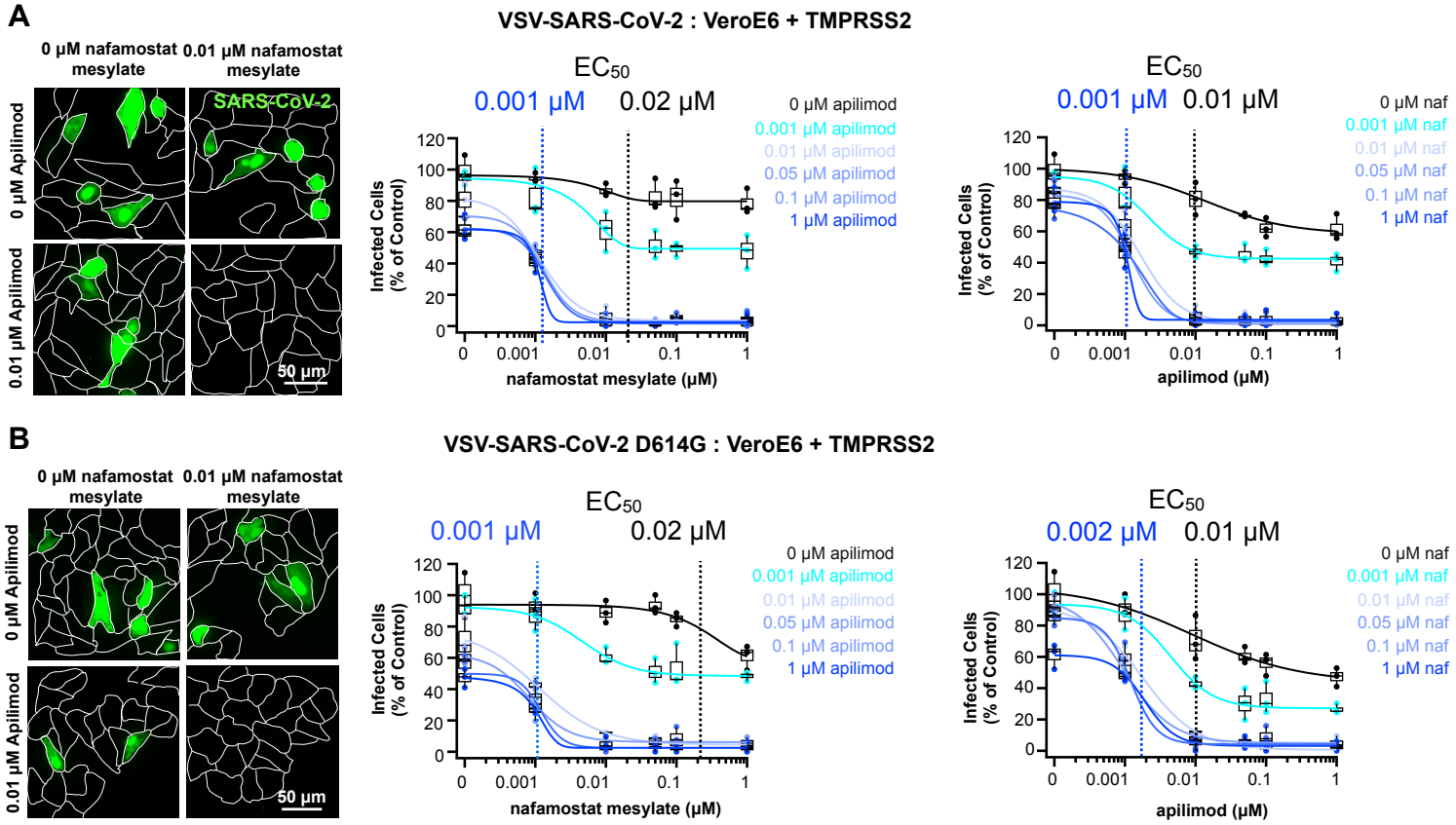
A
VSV-SARS-CoV-2 : VeroE6 + TMPRSS2
0 μM nafamostat mesylate
0.01 μM nafamostat mesylate
0 μM Apilimod
0.01 μM Apilimod
SARS-CoV-2
50 μm
EC50
0.001 μM
0.02 μM
0 μM apilimod
0.001 μM apilimod
0.01 μM apilimod
0.05 μM apilimod
0.1 μM apilimod
1 μM apilimod
Infected Cells (% of Control)
nafamostat mesylate (μM)
EC50
0.001 μM
0.01 μM
0 μM naf
0.001 μM naf
0.01 μM naf
0.05 μM naf
0.1 μM naf
1 μM naf
apilimod (μM)
B
VSV-SARS-CoV-2 D614G : VeroE6 + TMPRSS2
0 μM nafamostat mesylate
0.01 μM nafamostat mesylate
0 μM Apilimod
0.01 μM Apilimod
50 μm
EC50
0.001 μM
0.02 μM
0 μM apilimod
0.001 μM apilimod
0.01 μM apilimod
0.05 μM apilimod
0.1 μM apilimod
1 μM apilimod
Infected Cells (% of Control)
nafamostat mesylate (μM)
EC50
0.002 μM
0.01 μM
0 μM naf
0.001 μM naf
0.01 μM naf
0.05 μM naf
0.1 μM naf
1 μM naf
apilimod (μM)

**Figure 3**

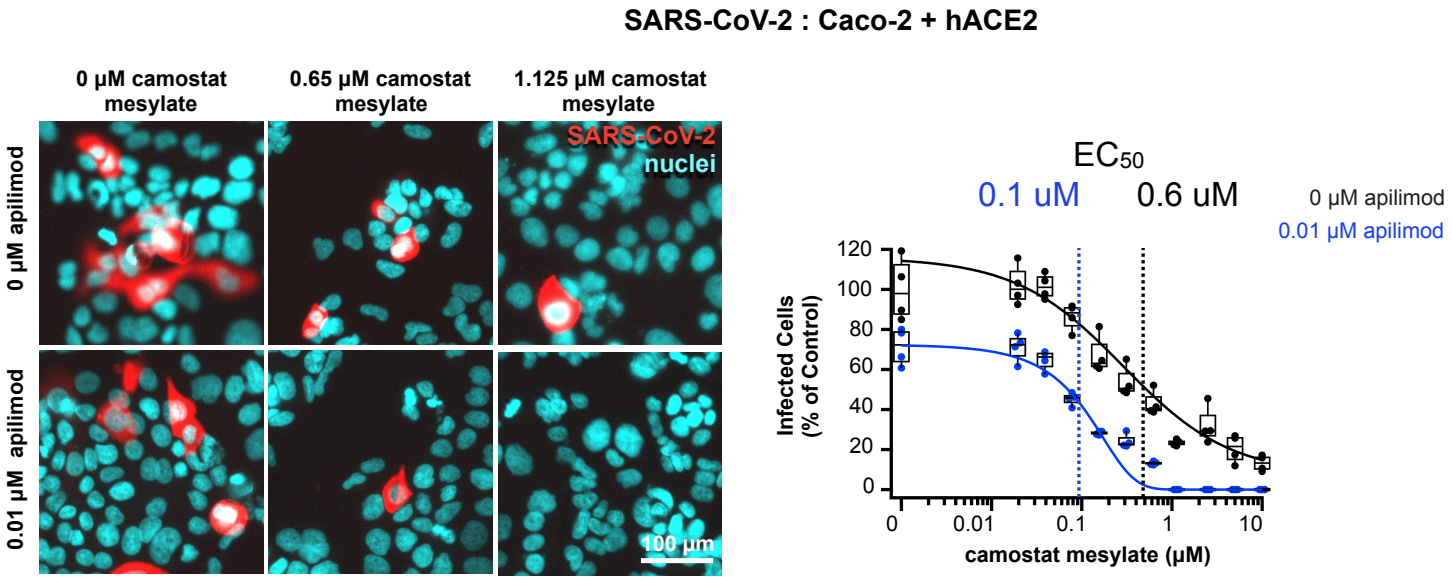
SARS-CoV-2 : Caco-2 + hACE2
0 µM camostat mesylate
0.65 µM camostat mesylate
1.125 µM camostat mesylate
0 µM apilimod
0.01 µM apilimod
SARS-CoV-2
nuclei
100 µm
EC50
0.1 uM
0.6 uM
0 µM apilimod
0.01 µM apilimod
Infected Cells (% of Control)
120
100
80
60
40
20
0
0
0.01
0.1
1
10
camostat mesylate (µM)

**Figure 4**